



Fast growth can counteract antibiotic susceptibility in shaping microbial community resilience to antibiotics

Daniel R. Amor^{a,1,2} and Jeff Gore^{a,1}

Edited by Jizhong Zhou, The University of Oklahoma, Norman, OK; received September 14, 2021; accepted March 1, 2022 by Editorial Board Member Simon A. Levin

Microbial communities often face external perturbations that can induce lasting changes in their composition and functions. Our understanding of how multispecies communities respond to perturbations such as antibiotics is limited, with susceptibility assays performed on individual, isolated species our primary guide in predicting community transitions. Here, we studied how bacterial growth dynamics can overcome differences in antibiotic susceptibility in determining community resilience: the recovery of the original community state following antibiotic exposure. We used an experimental community containing *Corynebacterium ammoniagenes* and *Lactobacillus plantarum* that displays two alternative stable states as a result of mutual inhibition. Although *C. ammoniagenes* was more susceptible to chloramphenicol in monocultures, we found that chloramphenicol exposure nonetheless led to a transition from the *L. plantarum*-dominated to the *C. ammoniagenes*-dominated community state. Combining theory and experiments, we demonstrated that growth rate differences between the two species made the *L. plantarum*-dominated community less resilient to several antibiotics with different mechanisms of action. Taking advantage of an observed cooperativity—a dependence on population abundance—in the growth of *C. ammoniagenes*, we next analyzed in silico scenarios that could compromise the high resilience of the *C. ammoniagenes*-dominated state. The model predicted that lowering the dispersal rate, through interacting with the growth at low population densities, could make the *C. ammoniagenes* state fragile against virtually any kind of antibiotic, a prediction that we confirmed experimentally. Our results highlight that species susceptibility to antibiotics is often uninformative of community resilience, as growth dynamics in the wake of antibiotic exposure can play a dominant role.

microbial communities | antibiotics | alternative stable states | resilience | community dynamics

Microbial communities often display alternative stable states that regulate their ecological functions (1–8). For example, while the human gut microbiome is stable to changes in daily life, exposure to strong perturbations can induce lasting shifts in its community composition, in turn leading to persistent changes in community functions (9, 10). Such is the case of *Clostridioides difficile* infections, which can opportunistically take over a gut community that has been compromised by antibiotic exposure (11). This shift toward a *C. difficile*-dominated community constitutes a switch toward an alternative, and unhealthy, stable state of the community that can be resilient to further antibiotic treatments. In soil microbiomes, human-driven leakage of antibiotics can cause lasting shifts in microbial community composition—e.g., changes in the fractions of Gram-positive bacteria and antibiotic resistant taxa—that can in turn compromise long-term soil productivity (12). Given their strong impact in human health and ecosystem functioning, understanding the drivers of regime shifts in microbial communities (13–17) is an important challenge.

Over the last 70 y, the use of antibiotics has been one of the most powerful tools in taming microbial pathogens (18). The use of this tool is guided by assays that measure the drug susceptibility of pathogen isolates (19), yet treatments generally expose not only the pathogen but also a broader host-associated bacterial community to the antibiotic (9, 20, 21). The resulting multispecies dynamics are difficult to predict, and expectations based on drug susceptibility can be misleading. Such complexities arise in part due to emergent properties of communities that allow microbes to either tolerate or deactivate the drug (22, 23). For instance, horizontal gene transfer can rapidly provide some pathogens with antibiotic resistance mechanisms (24). Microbial interactions (25) such as cross-protection due to active or passive inactivation of antibiotics by resistant strains frequently allow susceptible strains to survive drug exposure (26–29). The relative importance of antibiotic susceptibility over other microbial traits that can shape community dynamics after antibiotic exposure remains largely unknown.

Significance

Antibiotic exposure stands among the most used interventions to drive microbial communities away from undesired states. How the ecology of microbial communities shapes their recovery—e.g., posttreatment shifts toward *Clostridioides difficile* infections in the gut—after antibiotic exposure is poorly understood. We study community response to antibiotics using a model community that can reach two alternative states. Guided by theory, our experiments show that microbial growth following antibiotic exposure can counteract antibiotic susceptibility in driving transitions between alternative community states. This makes it possible to reverse the outcome of antibiotic exposure through modifying growth dynamics, including cooperative growth, of community members. Our research highlights the relevance of simple ecological models to better understand the long-term effects of antibiotic treatment.

Author contributions: D.R.A. and J.G. designed research, performed research, contributed new reagents/analytic tools, analyzed data, and wrote the paper.

The authors declare no competing interest.

This article is a PNAS Direct Submission. J.Z. is a guest editor invited by the Editorial Board.

Copyright © 2022 the Author(s). Published by PNAS. This article is distributed under Creative Commons Attribution-NonCommercial-NoDerivatives License 4.0 (CC BY-NC-ND).

¹To whom correspondence may be addressed. Email: daniel.amor@uni-graz.at or gore@mit.edu.

²Present address: Institute of Biology, University of Graz, Graz, A-8010 Austria.

This article contains supporting information online at <http://www.pnas.org/lookup/suppl/doi:10.1073/pnas.2116954119/-DCSupplemental>.

Published April 8, 2022.

Several microbial traits have been shown to influence community resilience, the ability to return to the initial state after a temporary perturbation (30, 31). Growth rates can play an important role when conditions become favorable after temporary perturbations, as the fastest responders have an advantage at repopulating the ecosystem (32–34). This can potentially increase the resilience of stable states dominated by fast growers. Beyond growth rates, community resilience depends on microbial interactions (35). Within a population, intraspecific interactions, such as cooperative growth, can determine population abundance thresholds separating the capability to recover from temporary harm versus population collapse (36). Interspecific interactions—interactions between different community members—also shape community resilience. Predominantly mutualistic communities can be relatively fragile, as the failure of the weakest member can strongly compromise the survival of the rest (37). While competitive interactions can potentially lead to higher resilience, competition can also increase the number of alternative stable states that the community can reach (7, 38, 39), potentially making transitions between such states more likely. There is a pressing need for a quantitative understanding of the interplay between community member traits and the kinds—and strengths—of perturbations that are required to steer microbial communities between alternative stable states.

Dispersal (40), the flux of individuals entering and leaving the community, can also play key roles in shaping microbial community stability and dynamics. Ingestion, for example, results in the frequent influx of large amounts of microbes into gut-associated communities, where the incoming cells interact with the resident microbiota influencing the overall community dynamics (41). A wealth of theoretical studies postulate that dispersal can enhance community richness and heterogeneity in ecological communities (42, 43), as well as promote regime shifts and fluctuations in species abundances (44–47). Not only this, but also dispersal is essential to reseed community members after local extinctions, which can dramatically increase community resilience (30). Over recent years, some of these theoretical predictions have been experimentally tested in both natural and synthetic microbial communities (48–53). The role of dispersal rates in driving the resilience of alternative stable states of microbial communities to antibiotic exposure is yet to be understood.

In recent work, we characterized a simple model community composed of two species, *Corynebacterium ammoniagenes* and *Lactobacillus plantarum*, that displays two alternative stable states. Both of these species are common in soils, and they are also among the culturable, human-associated microbiota (54). The genus *Lactobacillus* contains several probiotics, including *L. plantarum* (55), often considered beneficial for the host. Such a beneficial role might, however, depend on the ecological context, as members of this genus could also interfere with the recovery of microbial diversity—e.g. through acidification and metabolite production in the gut environment following antibiotic treatment (56). While the *Corynebacterium* genus has a number of human pathogens (57), *C. ammoniagenes* is considered a nonpathogenic species with potential use in the manufacture of prebiotics (58). In the laboratory, *C. ammoniagenes* and *L. plantarum* provide a minimal experimental model to study alternative stable states in microbial communities, as these species interact antagonistically through modifying the environmental pH in opposite directions (13, 38).

Here, we use the *C. ammoniagenes*–*L. plantarum* experimental community to study shifts between alternative stable states

after antibiotic exposure. While monocultures revealed that *C. ammoniagenes* was more susceptible to several antibiotics than its competitor *L. plantarum*, exposing the community to antibiotics resulted in shifts toward the stable state dominated by the more susceptible *C. ammoniagenes*. A simple theoretical model suggested that the most harmed species could still take over the system by growing faster than its competitor after the antibiotic was removed. Experimental measures over a range of experimental conditions verified the faster growth of *C. ammoniagenes*, while they also revealed signatures of cooperative growth. Incorporating cooperativity into the theoretical model predicted an interplay between cooperative growth and dispersal rate in driving community resilience. Indeed, lowering the experimental dispersal rate accentuated the effects of cooperative growth in *C. ammoniagenes*. In these conditions, a wide range of antibiotic perturbations involving different antibacterial mechanisms induced transitions toward the alternative stable state dominated by *L. plantarum*. Our results highlight that species susceptibility to antibiotics is often uninformative of community resilience, and ecological drivers such as cooperative growth and dispersal rates can play a much more dominant role after antibiotic exposure.

Results

As a model system to explore the resilience of alternative stable states to antibiotic exposure, we used a laboratory coculture of *L. plantarum* and *C. ammoniagenes*. These two species engage in a mutually inhibitory interaction (Fig. 1A) as a result of opposite and antagonistic modulation of the media pH (13, 38). When coculturing these bacteria under a serial dilution protocol, their mutual inhibition leads to two alternative outcomes in which one or the other species dominates the system. Moreover, applying a low dispersal rate of fresh cells daily during the serial dilutions does not affect the persistence of either outcome, indicating that the two outcomes constitute alternative stable states of the community (Fig. 1B). Beyond multistability, this experimental protocol captures some essential phenomena widely observed in microbial ecosystems (30): renewal of the populations via sequential episodes of death (dilutions) and regrowth, competitive interactions between community members, and arrival of new individuals through dispersal.

We next asked whether we could predict how antibiotic exposure induces transitions between the two stable states, based upon antibiotic susceptibility of the species. We found that *C. ammoniagenes* is significantly more susceptible than *L. plantarum* to the antibiotic chloramphenicol (Fig. 1C), with 3.1 $\mu\text{g}/\text{mL}$ chloramphenicol being sufficient to inhibit half-maximal growth of *C. ammoniagenes* over 24 h compared to 8.3 $\mu\text{g}/\text{mL}$ chloramphenicol for *L. plantarum*. The susceptibility of *C. ammoniagenes* to this antibiotic suggests that chloramphenicol might induce community shifts from the *C. ammoniagenes*-dominated state to the *L. plantarum*-dominated state. To test this hypothesis, we exposed each stable state of the community to 12.5 $\mu\text{g}/\text{mL}$ chloramphenicol for one daily cycle. Contradicting the susceptibility-based hypothesis, exposing the community to chloramphenicol revealed that the stable state dominated by the most susceptible species (*C. ammoniagenes*) is resilient to this perturbation—the community returned to its original stable state after the removal of the antibiotic (Fig. 1D and *SI Appendix, Fig. S1*). In contrast, the *L. plantarum*-dominated state is fragile against this perturbation: The community experienced a transition from the *L. plantarum*-dominated state to the *C. ammoniagenes*-dominated

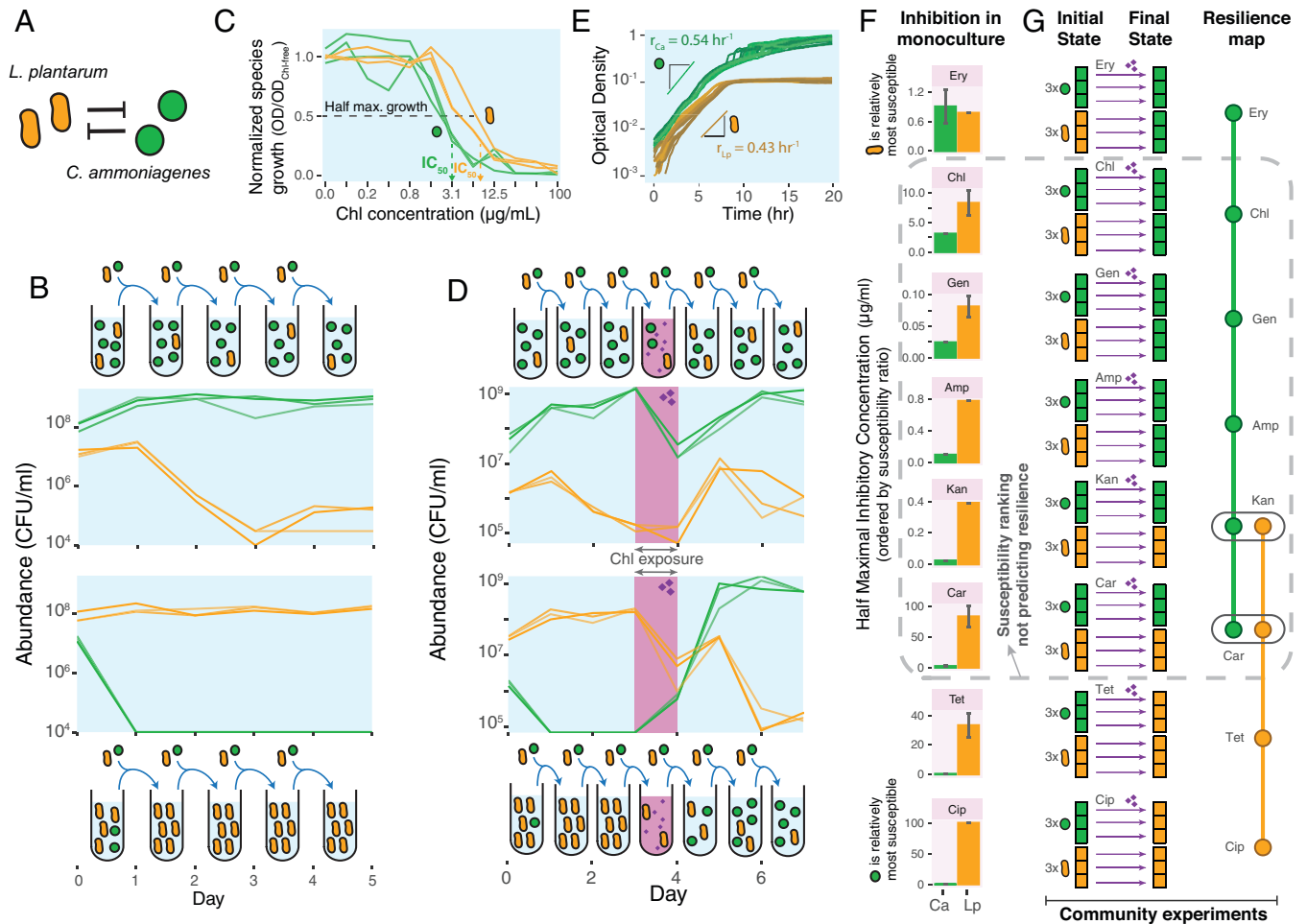


Fig. 1. Antibiotic susceptibility ranking fails to predict the outcome of antibiotic exposure in a bistable community. (A) The two species *L. plantarum* (orange) and *C. ammoniagenes* (green) exhibit mutually inhibitory interactions. (B) Coculturing *C. ammoniagenes* and *L. plantarum* under a serial dilution protocol including dispersal reveals two alternative stable states in which either species outcompetes the other. Green (orange) curves show the *C. ammoniagenes* (*L. plantarum*) abundance in coculture over five cycles of growth and 30-fold dilution with dispersal (10^5 fresh cells per [210 μ L] culture per day for each species, $n = 3$). Cartoons illustrate the experimental protocol and observed community dynamics. (C) *C. ammoniagenes* is more susceptible to chloramphenicol than *L. plantarum*. Shown is 24-h growth of monocultures of each species ($n = 3$) in the presence of chloramphenicol at different concentrations (normalized by the average growth in the absence of antibiotic). IC_{50} is measured as the average minimum concentration that inhibits growth by at least 50% (SI Appendix, Fig. S3 shows that our results are qualitatively robust to measuring IC_{50} via growth rate reduction). (D) The stable state dominated by *C. ammoniagenes* is the most resilient to chloramphenicol exposure. The time series shows the response of the community (monitored through species abundances) to temporary exposure to chloramphenicol. Top (Bottom) panel shows the results for three replicate cocultures starting from the stable state dominated by *C. ammoniagenes* (*L. plantarum*). Color scheme is as in B; pink color highlights the 24-h cycle under antibiotic exposure. (E) *C. ammoniagenes* exhibits a higher growth rate than *L. plantarum*. Shown is the time series for the optical density of each species in monoculture ($n = 24$). (F) Susceptibility (IC_{50}) of *C. ammoniagenes* and *L. plantarum* to eight different antibiotics (mean \pm SEM, $n = 3$). Data are ordered by susceptibility ratio: (Top) *L. plantarum* shows the highest susceptibility relative to the susceptibility of *C. ammoniagenes*. (G) Resilience of each stable state of the community to antibiotic exposure. Color-coded squares show the stable state reached by the community before (initial state) and after (final state) exposure to the indicated antibiotic ($n = 3$). (Right) The subway plot indicates the states that are resilient to each antibiotic perturbation. The dashed rectangle highlights the five cases in which predictions based on species susceptibility do not agree with the observed resilience. Ca, *C. ammoniagenes*; Lp, *L. plantarum*. Ery, erythromycin; Chl, chloramphenicol; Gen, gentamicin; Amp, ampicillin; Kan, kanamycin; Car, carbenicillin; Tet, tetracycline; Cip, ciprofloxacin.

one as a result of chloramphenicol exposure. Starting from the stable state dominated by *L. plantarum*, antibiotic exposure led to a significant decrease in the overall cell abundance reached at the end of the exposure cycle, although no change in species abundance rank occurred until 1 d later—when *C. ammoniagenes* took over the community. The fact that *C. ammoniagenes* increased its abundance from day 3 to day 4 is consistent with chloramphenicol attenuating the competitive effect of *L. plantarum* through reducing its effective growth during the exposure cycle. In the absence of antibiotic, a dominant population of *L. plantarum* effectively leads to extinction of *C. ammoniagenes* cells ($\sim 10^5$ colony-forming units [CFU] per culture) that arrive through dispersal at the beginning of each cycle, but in the presence of chloramphenicol such cells can survive—even if they exhibit

little or no growth during the antibiotic exposure cycle. Species susceptibility to chloramphenicol was therefore insufficient to predict the direction of community shifts following antibiotic exposure.

In the search for species traits beyond antibiotic susceptibility that could shape community resilience, we measured the exponential phase growth rate of each species. We found that *C. ammoniagenes*, the most susceptible species (Fig. 1C), is also the fastest grower of the two species (Fig. 1E). We hypothesized that the observed growth rate ranking could counteract the ranking of susceptibilities in shaping community resilience to antibiotics: While a higher susceptibility could make the *C. ammoniagenes*-dominated state more fragile against antibiotic exposure, a higher species growth rate could also allow the *C. ammoniagenes* population to recover faster after

perturbations. Noting that this simple hypothesis does not invoke specific antibiotic mechanisms of action, we next studied both the susceptibility ranking and the community outcome of temporary drug exposure for a range of antibiotics spanning several mechanisms of action (Fig. 1 *F* and *G* and *SI Appendix*, Figs. S2 and S3). As expected, when the fast-growing *C. ammoniagenes* species was also the less susceptible species (as was the case for erythromycin), we observed that antibiotic exposure results in transitions toward the *C. ammoniagenes*-dominated state (Fig. 1 *F* and *G*, *Top*). On the other hand, in cases where *C. ammoniagenes* was much more susceptible to the antibiotic (ciprofloxacin and tetracycline) we observed transitions to the *L. plantarum*-dominated state (Fig. 1 *F* and *G*, *Bottom*). In addition, we found five antibiotics for which the susceptibility ranking favored *L. plantarum*, and yet community resilience varied from both stable states being resilient—kanamycin and carbenicillin—to only the state dominated by the faster-growing *C. ammoniagenes* being resilient—chloramphenicol, gentamycin, and ampicillin. These observations were consistent with our hypothesis that differences in species growth rates can counteract differences in antibiotic susceptibility in shaping community resilience.

To gain understanding of how the interplay between species susceptibility and growth rates determines community resilience against antibiotics, we employed a Lotka–Volterra interspecific competition model, modified to include dispersal of cells as well as antibiotic-induced death:

$$\begin{aligned} \frac{dF}{dt} &= r_F F(1 - F - \alpha_{FS} S) + D - \delta_F(t) F, \\ \frac{dS}{dt} &= r_S S(1 - S - \alpha_{SF} F) + D - \delta_S(t) S. \end{aligned} \quad [1]$$

F and S are the normalized abundances of a fast-grower and a slow-grower species, respectively; r_F and r_S are the maximum per capita growth rates of each species; α_{FS} and α_{SF} capture the strength of interspecies inhibition; D is the dispersal rate that captures the arrival of fresh cells into the system; and $\delta_F(t)$ and $\delta_S(t)$ are the antibiotic-associated death rates of each species. In the absence of both dispersal and antibiotics [$D = \delta_F(t) = \delta_S(t) = 0$] we recover the competitive Lotka–Volterra model, in which the outcome is bistable if $\alpha_{FS} > 1$ and $\alpha_{SF} > 1$. In agreement with our experimental protocol, we assume that the dispersal rate D is identical for the two species. The mortality rates $\delta_F(t)$ and $\delta_S(t)$ capture differences in the susceptibilities of the species to temporary antibiotic exposure (Fig. 2 *A* and *B*).

The modified Lotka–Volterra model predicts that differences in both susceptibility and growth rate shape community resilience against temporary antibiotic exposure. During a given perturbation, the decrease in each normalized species abundance during antibiotic exposure depends on its susceptibility (added death rate in the model), and the recovery dynamics of each species in the wake of antibiotic exposure are highly dependent on its maximum per capita growth rate—either species needs to grow to a significantly high normalized abundance before the nonlinear interaction term becomes high enough to effectively inhibit the competitor species. The phase diagrams in Fig. 2 *B* and *SI Appendix*, Figs. S4–S6 show that, through changing either the species growth rate ratio or the susceptibility ratio, the community outcome of antibiotic exposure can change from transitioning to the stable state dominated by the fast grower to transitioning to the stable state dominated by the slow grower. The former case reveals a higher resilience of the stable state dominated by the fast grower, while the latter reveals fragility of this state against the perturbation. In

between these two regimes, there is a region where both stable states are resilient to the perturbation and no transitions between alternative stable states follow antibiotic exposure. This simple model is therefore able to recapitulate the core experimental outcomes observed in our community exposed to different antibiotics: The more susceptible species can still take over the community after antibiotic exposure if its relative growth rate is fast enough.

A minimal strength—intensity—of any given perturbation is known to be necessary to meaningfully impact an ecological community, and this includes antibiotic perturbations to microbial communities. Indeed, our model predicts that after weak perturbations in which none of the species are dramatically harmed, the community can recover its original stable state (Fig. 2 *C*). As the strength of the perturbation (antibiotic-associated death rate) increases, one of the stable states becomes fragile and transitions to the more resilient state occur. To test this prediction experimentally, we temporarily exposed each stable state of the community to a range of chloramphenicol concentrations (Fig. 2 *D* and *SI Appendix*, Fig. S7). In agreement with the theoretical prediction, we observed that transitions between stable states following chloramphenicol exposure occur only after crossing a threshold ($\sim 6.2 \mu\text{g/mL}$) in antibiotic concentration.

To validate the hypothesis that species growth rates could drive community resilience in the experiments, we next asked whether we could also manipulate the growth rate ratio between the two species. In previous work we demonstrated that the mutually inhibitory interaction between the two species is due to an antagonistic feedback with the environmental pH (13, 38). While *C. ammoniagenes* alkalizes the environment—which favors its own growth and inhibits the growth of its competitor, *L. plantarum* acidifies the system—which has opposite effects to those of alkalization (Fig. 3 *A* and *SI Appendix*, Fig. S8). Given the cooperative nature of these processes, where a higher number of cells should more efficiently modify the pH and, consequently, its own growth rate, we next looked for signatures of cooperative growth in each species. Cooperative growth, also known as the Allee effect (59), implies a decrease in the per capita growth rate at low cell densities. We observed that *C. ammoniagenes*, in addition to being a faster grower, also displayed a significant abundance dependence in its growth, while the growth of *L. plantarum* is relatively independent of cell abundance (Fig. 3 *B*). The observed cooperative growth in *C. ammoniagenes* suggested that the relative growth rates of the two species could potentially be altered in experimental scenarios where cell populations fall below a given abundance threshold.

To better understand the impact of cooperative growth on community resilience, we modified the theoretical model to account for an abundance-dependent per capita growth rate. In particular, we modified the equation for the dynamics of F as

$$\frac{dF}{dt} = r_F F \left(\frac{F}{a + F} (1 - F) - \alpha_{FS} S \right) + D - \delta_F(t) F, \quad [2]$$

where the parameter a introduces an Allee effect. For the case of monocultures—species growing in isolation with no dispersal and no antibiotic—at high cell densities F still grows faster than S (Fig. 3 *C*). At low population densities, F experiences a decrease in the per capita growth rate that leads to a switch in the growth rate ranking of the two species. Simulating the effects of antibiotic exposure in coculture scenarios revealed that the impact of the Allee effect on community dynamics

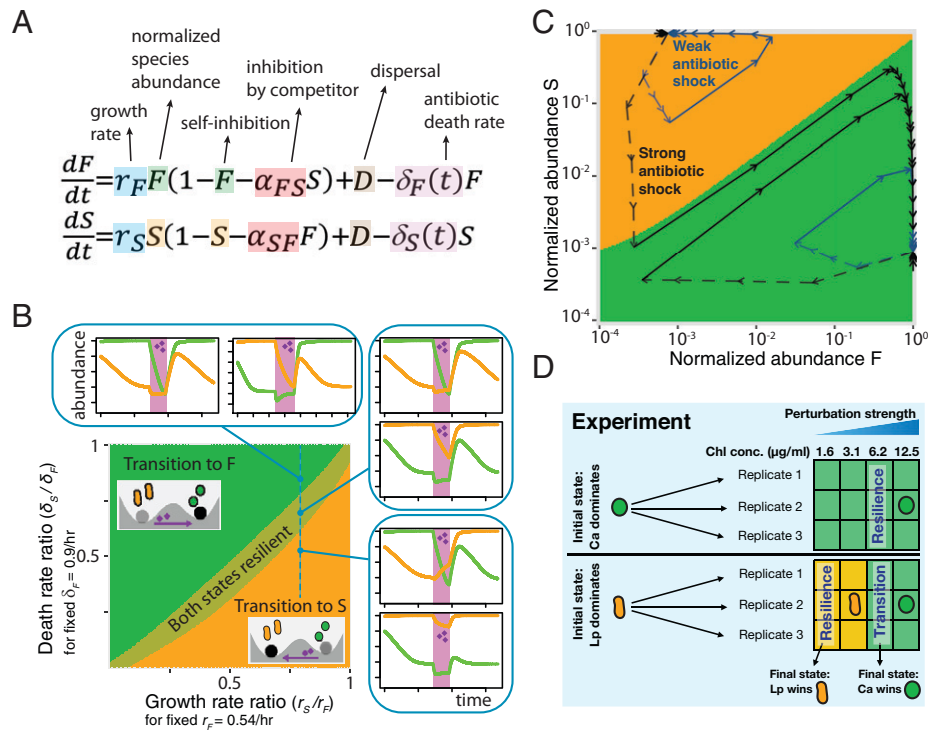


Fig. 2. Fast growth can counteract antibiotic susceptibility in shaping community resilience to antibiotics. (A) Minimal theoretical model to study resilience to antibiotic exposure in two-species communities. (B) Phase diagram, and representative time series, showing the outcome of antibiotic exposure in the model. Horizontal (vertical) axis shows the relative growth (death) rate of species *S* relative to that of species *F*. For similar susceptibilities (added death rates) but significantly different growth rates, the most resilient state is dominated by the fast grower (green region). In contrast, transitions to the state dominated by the slow grower (orange region) are observed for similar growth rates but significantly different susceptibilities. In between the two scenarios, there is a parameter region (olive green) in which both states are resilient to antibiotic exposure. The basins of resilience are representative of the three qualitative regimes of the community, although the exact position of the interface between regimes depends on the maximum values of r_F and δ_F . Analogously, these three basins of resilience are qualitatively, although not quantitatively, robust to explicitly modeling differences in interaction strengths and carrying capacities (SI Appendix, Fig. S4). (C) Phase diagram indicating the stable state reached by simulated cocultures starting at the indicated abundances. Arrows show the trajectories of communities that start close to either stable state and experience the added death rates that simulate temporary antibiotic exposure (dashed arrows show the trajectories during the simulated antibiotic exposure). Different perturbation strengths correspond to different values for the magnitude of the added death rates while keeping their ratio constant (Materials and Methods). (D) A minimum strength (antibiotic concentration) of the perturbation is needed to experimentally observe transitions between stable states. From an initial state dominated by either species (Top, *C. ammoniagenes* in green; Bottom, *L. plantarum* in orange), the matrix shows the final stable state reached by each of three replicate cocultures (rows) that were temporarily exposed to different chloramphenicol concentrations (columns). Ca, *C. ammoniagenes*; Lp, *L. plantarum*.

depends on the dispersal rate. This is because the dispersal rate, the number of fresh cells that enter the system per unit time, plays a key role in determining how low the population abundance can fall during antibiotic exposure (SI Appendix, Fig. S9), which strongly affects the dynamics of the species subject to abundance-dependent growth. As a result, when accounting for an Allee effect acting on the fast-grower species, the model predicts that lowering the dispersal rate can change the ratio of species growth rates in the wake of antibiotic exposure, reducing the resilience of the state dominated by the species subject to an Allee effect (Fig. 3D and SI Appendix, Fig. S9).

To test this prediction experimentally, we temporarily exposed either stable state of the community to chloramphenicol under a lower dispersal rate (Fig. 3E and SI Appendix, Fig. S10). In this case, after the total cell abundance decreased due to chloramphenicol exposure, the fraction of the population shifted toward *L. plantarum* dominance, regardless of the initial state. When we repeated the same experiments using seven different antibiotics, we observed that the *C. ammoniagenes*-dominated stable state was no longer the most resilient across different antibiotics (Fig. 3F and SI Appendix, Fig. S11). While in the first set of experiments the stable state dominated by *C. ammoniagenes* was resilient to six of eight antibiotics (Figs. 1G and 3F), lowering the experimental dispersal rate by an order of magnitude dramatically decreased the

resilience of this stable state. Under this lower dispersal rate, all eight antibiotics, independent of the species susceptibility ranking, induced transitions toward the alternative stable state dominated by the competitor species *L. plantarum*. In agreement with the theoretical prediction, these experimental results show that the Allee effect can dramatically reduce the resilience of a community to antibiotic perturbations.

Discussion

Our results highlight the important role of growth traits of community members in shaping the resilience of microbial communities to antibiotic perturbations. In particular, we have shown that differences in the growth rate of community members can drive transitions between alternative stable states in the wake of antibiotic exposure and that these differences can be subject to abundance-dependent growth effects—such as intraspecific cooperation. Moreover, the impact of growth traits on community dynamics after antibiotic exposure can be largely independent of specific antibiotic mechanisms: Our experiments, guided by a simple theoretical model, revealed that fast growth can counteract antibiotic susceptibility in shaping community resilience over a wide range of antibiotic classes. For fixed growth rates, the ratio of species susceptibilities has to cross a given threshold to become the main driver of

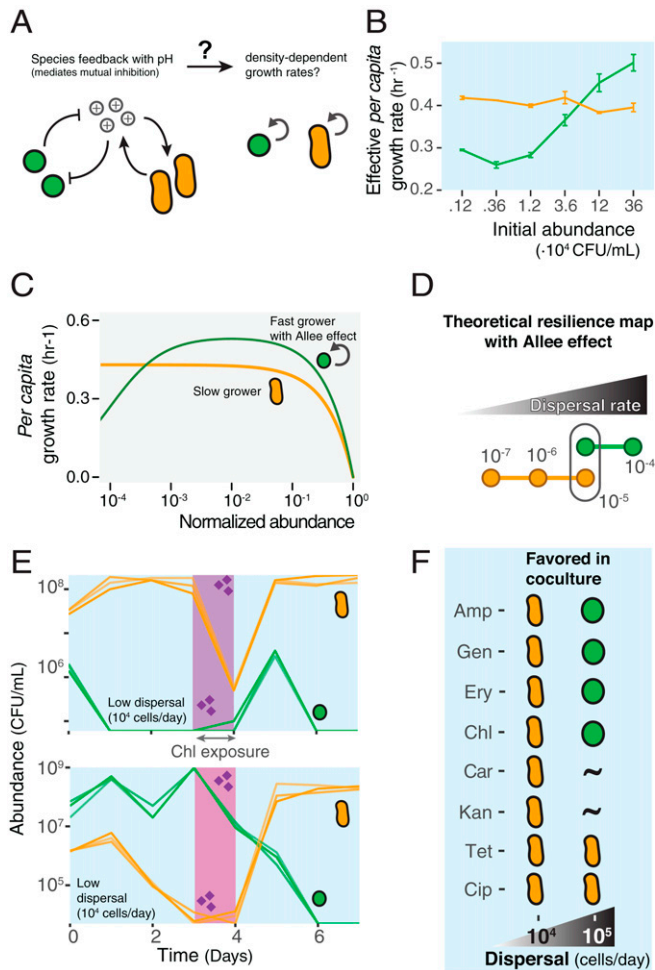


Fig. 3. An interplay between abundance-dependent growth and dispersal can drive community shifts in the wake of antibiotic exposure. (A) Feedback loops between the growth of the two species and environmental pH suggest that these species could exhibit abundance-dependent growth. (B) *C. ammoniagenes* exhibits abundance-dependent growth. Shown is effective growth rate of monocultures inoculated at different initial cell densities (mean \pm SEM, $n = 3$), *C. ammoniagenes* in green and *L. plantarum* in orange. (C) Per capita growth rate of a fast-grower subject to an Allee effect (green) and a slower-growing species (orange) as a function of normalized abundance, both species under logistic growth. (D) Subway plot for the predicted dispersal dependence of community resilience after accounting for an Allee effect on species *F* in the theoretical model. (E) Time series for the observed species abundances as either stable state is temporarily exposed to 12.5 $\mu\text{g/mL}$ of chloramphenicol under low (10^4 cells per day) dispersal rate. (F) For eight different antibiotics, lowering the dispersal rate increases the resilience of the stable state dominated by *L. plantarum*. Cell cartoons indicate the dominant species in the experimental outcome of temporarily exposing the community to the indicated antibiotic (rows) under the indicated dispersal rate (columns). The ~ symbol indicates that no transitions between stable states were observed.

community resilience (Figs. 1 *F* and *G* and 2*B*). Together with recent works revealing additional community-emergent mechanisms (27–29) that shape microbial community resilience, our findings highlight the limitations of monoculture susceptibility assays when trying to predict the response of a community to antibiotics.

Antibiotic-resistant bacteria can play a major role in driving community dynamics following antibiotic exposure. In our experiments, we used nonengineered strains lacking any experimentally added plasmids or chromosomal integrations that could provide resistance. Susceptibility assays showed that *C. ammoniagenes* is generally sensitive to the antibiotics that we tested; it exhibits significant growth reduction in $\sim 3\mu\text{g/mL}$ of

drugs that inhibit protein synthesis via binding to the ribosomal RNA complex at the 50S subunit—such as chloramphenicol and erythromycin—and even lower concentrations of drugs targeting other subunits in the ribosomal RNA complex—cases for gentamycin and kanamycin—as well as DNA-gyrase inhibitors such as ciprofloxacin. In turn, *L. plantarum* exhibited a broader range of susceptibilities, exhibiting relatively high susceptibility to kanamycin and erythromycin and virtually no susceptibility to ciprofloxacin (an antibiotic to which *L. plantarum* is known to be naturally resistant) (60). As expected, resistance confers a strong advantage to *L. plantarum* in the event of antibiotic exposure, which is consistent with the theoretical prediction that extreme ratios of susceptibilities can offset the importance of growth rate differences between community members (Fig. 2*B*). Over longer timescales and with multiple antibiotic exposures, it would also be important to consider how evolutionary adaptations alter the resilience of community states.

In a community, interactions between any given species and antibiotics can lead to counterintuitive outcomes. For example, cross-protective interactions can emerge when a species can effectively reduce the bioavailability of antibiotics in a way that benefits other members of the community. Either active (e.g., enzymatic antibiotic degradation) (26, 29) or passive (e.g., via absorption into cells or binding to cell membranes) (28) reduction in antibiotic bioavailability has been shown to drive community dynamics in different scenarios. In the case of our model community, spent media experiments revealed that *C. ammoniagenes* populations can offer modest protection to *L. plantarum* against some antibiotics, especially the beta-lactams ampicillin and carbenicillin (SI Appendix, Figs. S12 and S13). This result is consistent with recent findings that binding, followed by deactivation, of beta-lactams by one species can benefit a competitor species (28). This kind of protection was observed only when *C. ammoniagenes* populations exceed a given threshold in abundance: While bulk populations from the *C. ammoniagenes*-dominated state could lead to modest protection to both *C. ammoniagenes* and *L. plantarum* cells against beta-lactams, we did not detect significant protection from either *L. plantarum* populations (that exhibit lower abundance than *C. ammoniagenes* populations; SI Appendix, Fig. S12) or dispersal-associated cell populations (SI Appendix, Fig. S13). Such cross-protective interactions could therefore compromise the resilience of the *C. ammoniagenes*-dominated community state, since *C. ammoniagenes* is both the most susceptible species and the one exhibiting some degree of cross-protection toward *L. plantarum*. Despite this disadvantage of the *C. ammoniagenes*-dominated state, under the standard dispersal rate in Fig. 1, this state was resilient to most of the antibiotic perturbations. The fact that the dispersal rate, through interacting with the growth of *C. ammoniagenes* at low abundances, qualitatively changed community resilience to six of eight different antibiotics, with only the two cases in which the susceptibility ratio was most favorable to *L. plantarum* remaining unaffected, suggests that cross-protection does not play a major role in determining community resilience in our experiments. We also confirmed that the media pH remained effectively independent of the addition of antibiotics in our experiments, since it could otherwise affect community resilience by interfering with the pH-driven ecological interaction between the two species. These results are consistent with the dominant role of species growth rate differences as drivers of resilience in the *C. ammoniagenes*–*L. plantarum* community. Future work should address the importance of

growth rate differences relative to other ecological drivers of resilience in different microbial communities and scenarios.

For simplicity and clarity, our theoretical analysis was built around a simple phenomenological model of interspecies interactions and antibiotic inhibition. This approach allowed us to make qualitative predictions across a wide range of antibiotics, but we have also confirmed that the core predictions can be recapitulated in mechanistic models incorporating particular modes of action of antibiotics, such as for bacteriostatic inhibition of cell division by chloramphenicol (*SI Appendix, Fig. S14*). We used the competitive Lotka–Volterra model to predict qualitatively different regimes of community resilience to antibiotics without the need to account for very specific details of the experimental system, such as finely tuning interspecies interaction strengths, carrying capacities, or discrete dilutions, although the predicted phases of resilience are robust to changes in these different features of the model (*SI Appendix, Figs. S4 and S14*). Future work could explore the impact of additional growth traits on community resilience, such as the effects of lag times—following antibiotic removal and also nutrient renewal during dilutions—and population heterogeneity in response to antibiotics (61).

Although we did not address more diverse communities experimentally, we extended our model to study the role of growth rates in shaping the resilience of alternative stable states in diverse communities. We simulated communities containing two groups of 10 species displaying strong intergroup inhibition and found that community resilience depends on average susceptibilities and average growth rates (*SI Appendix, Fig. S15*). Consistent with our results in simple experimental communities, groups of species are generally more resilient as either their average growth rate increases or their average susceptibility decreases. Further extensions of the model, and experiments, should also address whether this generic trend holds under different environments, such as within a host organism. The immune system of a host, for example, can play a major role in promoting, or inhibiting, the growth of different microbial taxa via environmental filtering. Nonetheless, generic ecological trends observed *in vitro*, e.g., simple rules for community assembly, have also been shown to be informative with relative independence of the immune system in simple experimental hosts such as nematodes (62).

Research in probiotics aims to find dispersal-based ways, through increasing the intake rate of specific taxa, to increase the resilience of gut community states most associated to health. Our results suggest that, beyond tuning the ratio at which community members enter an ecosystem, the overall rate of dispersal could also lead to alternative community outcomes. Persistent *C. difficile* infections also exhibit potential parallels to our observation of dispersal-dependent resilience. While diet-driven dispersal rates can be insufficient to prevent a recurrent *C. difficile* infection after antibiotic treatments, fecal transplants—a massive dispersal event from a healthy community—are most effective in leading the gut microbiota to a successful recovery. Overall, our results highlight that ecological approaches that account for relatively simple traits of community members can improve predictions of microbial community response to antibiotics.

Materials and Methods

Laboratory Strains. *L. plantarum* (American Type Culture Collection [ATCC] 8014) and *C. ammoniagenes* (ATCC 6871) were obtained from ATCC.

Liquid Media, Agar Plates, and Culturing Conditions. Overnight precultures were performed in nutrient media (38): 10 g/L of yeast extract and 10 g/L of soytone (both from Becton Dickinson), pH 7. The experiments were performed in supplemented base media (SBM) (38). The stock of base media was prepared as 1 g/L yeast extract, 1 g/L soytone, 10 mM sodium phosphate buffer, 0.1 mM CaCl₂, 2 mM MgCl₂, 4 mg/L NiSO₄, 50 mg/L of MnCl₂, 1× Trace Metals Mixture (Teknova), and 10 mM sodium phosphate, pH adjusted to 6.5. SBM was prepared daily by supplementing base media with 10 g/L glucose and 8 g/L urea. All media were filter sterilized using the VWR Bottle Top Filtration Unit.

Plating was performed on Tryptic Soy Broth (TSB) (Teknova) with 2.5% agar (Becton Dickinson) in which we adjusted the pH to different values for selective plating (see below). Before plating for CFU counting, experimental cultures were diluted in phosphate-buffered saline (PBS) (Corning).

Before starting experiments, samples of bacterial isolates were thawed and streaked in TSB agar plates (pH 7) and incubated at 30 °C for 48 h. Individual colonies were then picked from these plates to start overnight precultures, which took place in 5 mL nutrient media, inside 50-mL Falcon tubes for 24-h shaking at 250 rpm on a New Brunswick Innova 2100 shaker (Eppendorf). Experimental cultures took place in 96-deepwell plates covered with AeraSeal adhesive sealing films (Excell Scientific), shaking at 1,350 rpm on a Heidolph platform shaker (Titramax 100; Heidolph North America). All precultures and cultures were incubated at 30 °C, relative humidity 50%.

Experimental Cocultures, Daily Dilutions, Dispersal, and Antibiotic Exposure. Overnight precultures of both *C. ammoniagenes* and *L. plantarum* were washed in 15 mL of base media and their cell abundance was adjusted so that they exhibit an optical density (OD)/cm of ~2.0. To begin an experiment, we mixed the two OD-adjusted populations at the target initial ratio (e.g., 95% of one species and 5% of the other, in volume) and inoculate 3 μL of the mix into a single well of the experimental plate containing 207 μL of fresh SBM.

At the end of every daily cycle, a 30-fold dilution was applied by transferring 7 μL of the experimental cultures into 203 μL of fresh SBM using a Vialflo 96-well pipettor (Vialflo settings: Pipette-Mix program, aspirating 7 μL, three mixing cycles, mixing volume 10 μL, speed 6).

To apply the daily dispersal, we washed fresh overnight precultures and adjusted their OD to 2.0 as indicated above. Then we performed a second round of adjustment of cell abundance to a final OD/cm of 0.37 for *C. ammoniagenes* and 0.24 for *L. plantarum*. We then mixed 10 mL of each monoculture, resulting in 20 mL of the migrant cells mix. Using a Vialflo 96-well pipettor, 3 μL of the migrant mix were inoculated into the (210 μL) experimental cultures right after each dilution cycle (Vialflo settings: Pipette-Mix program, aspirating 3 μL, three mixing cycles, mixing volume 10 μL, speed 6). This resulted in a daily inoculation of $(1.2 \pm 0.1) \cdot 10^5$ fresh cells from each species into the culture (13). For the low-migration ($\sim 10^4$ cells per day for each species) condition considered in Fig. 3 E and F, the migrant cells mix was 10× diluted before inoculation into the experimental plates.

For the experiments involving community exposure to antibiotics, the SBM in the experimental plate for day 3 was supplemented with the indicated antibiotic concentration before the daily dilution took place.

Estimation of Population Densities (CFU/mL). For CFU counting, 10-μL droplets of PBS-diluted cultures were plated on TSB agar. We used agar plates at pH 5 for selective plating of *L. plantarum* and at pH 10 to select for *C. ammoniagenes* colonies.

To prepare the 10-μL droplets, we serially diluted the experimental cultures via 10-fold dilutions (maximal dilution factor was 10^{-7}) using a 96-well pipettor (Vialflo 96; Integra Biosciences), using the program “pipet/mix” (pipetting volume, 20 μL; mixing volume, 180 μL; mixing cycles, 5; mixing and pipetting speed, 8). The 10-μL droplets were then transferred to 150-mm diameter agar plates with the 96-well pipettor (program “reverse pipette”: uptake volume, 20 μL; released volume, 10 μL; pipetting speed, 2). Droplets were allowed to dry and the plates were incubated at room temperature for 1 to 2 d until colonies were visible. The different dilution steps allowed us to find a dilution at which colonies could be optimally counted with a Leica dissecting microscope (between ~5 and ~50 colonies). Up to three plating replicates per condition were performed to increase accuracy at measuring population densities.

pH Measurement. After performing the daily dilution, 130- μL samples of the saturated cultures were transferred into 96-well PCR plates (VWR) and the pH was measured using a pH microelectrode (Orion, PerpHect, ROSS).

Antibiotic Susceptibility Measurements (Half-Maximal Inhibitory Concentration). To measure the half-maximal inhibitory concentration (IC_{50}) of the different antibiotics for each species, we prepared a series of $2\times$ dilutions of the antibiotic in SBM. The maximum concentration of antibiotic was 25 $\mu\text{g}/\text{mL}$ for both kanamycin and gentamycin and 100 $\mu\text{g}/\text{mL}$ for each of the other six antibiotics. A total of 207 μL of the antibiotic solutions was then transferred to a 96-well plate (300 μL capacity; VWR) where 3 μL of a monoculture of either *C. ammoniagenes* or *L. plantarum* was inoculated. Each inoculum contained $\sim 10^6$ cells that were prepared through washing and diluting overnight precultures as described above. The 96-well plate was incubated at 30 $^\circ\text{C}$ with shaking in a Tekan Infinite M200Pro plate reader, and OD 600-nm measurements were taken every 15 min. We determined the IC_{50} of each antibiotic for each bacterial species as the minimal concentration that reduced growth by at least 50% of the antibiotic-free growth after 24 h (taking in each case the average IC_{50} of three replicate experiments).

Maximum Growth Rates and Allee Effect. To measure growth rates in the absence of the antibiotics (Fig. 1E), monocultures of *C. ammoniagenes* and *L. plantarum* were prepared and incubated as for the IC_{50} measurements, but in antibiotic-free conditions. We used eight technical replicates for each species and repeated the experiment three times, leading to the 24 growth time series in Fig. 1E. Maximum growth rates were obtained by fitting an exponential growth rate to the data for each monoculture within the OD range 10^{-2} to $5\cdot 10^{-2}$ cm^{-1} , and then we computed the average over all replicates for each species.

To measure the Allee effect (Fig. 3B) we prepared an initial population of 10^6 cells as described above and also a range of initial population densities obtained through additional dilution steps. We also measured the OD of a 10^7 cells population prepared in identical conditions and used its OD value to compute the expected initial OD of all the initial populations in the experiment (for which the initial OD was near or below the detection limit). The resulting monocultures covering a range of initial cell densities were incubated in a plate reader in the same conditions described above for the maximum growth rates measurements. The effective growth rate in Fig. 3B was computed through the ratio $\log(\text{OD}_{\text{threshold}} / \text{OD}_i) / T_{\text{threshold},i}$ where $T_{\text{threshold},i}$ is the time that each population

took to reach an optical density threshold $\text{OD}_{\text{threshold}} = 10^{-2}$ cm^{-1} , and OD_i is the initial OD of that population.

Simulations. The set of equations in [1] and its extension in [2] were numerically solved in R using the differential equation solver `ode()` in the `deSolve` library. Unless stated otherwise, all numerical simulations used the parameter values

$$\left\{ \begin{array}{l} r_f = 0.54 \text{ [h}^{-1}\text{]} \\ r_s = 0.43 \text{ [h}^{-1}\text{]} \\ \alpha_{FS} = \alpha_{SF} = 1.25 \\ D = 10^{-4} \text{ [h}^{-1}\text{]} \\ \delta_f = 0.9 \text{ [h}^{-1}\text{]} \text{ if } 72 < t < 96 \\ \delta_s = 0.7 \text{ [h}^{-1}\text{]} \text{ if } 72 < t < 96 \\ a = 10^{-4}, \end{array} \right.$$

where the condition for the added death rates δ_f and δ_s means that the corresponding death rates were applied only temporarily within the interval $t \in [72, 96]$ simulated hours and were both equal to zero otherwise.

To vary the growth rate ratio in Fig. 2B, we kept constant the growth rate $r_f = 1.0$ as we decreased the value of r_s . To vary the death rate ratio in Fig. 2B, we kept constant the death rate of $\delta_f = 1.3$ as we decreased the value of δ_s . The weak antibiotic shock in Fig. 2C was implemented using $\delta_f = 0.65$ and $\delta_s = 0.5$.

Data Availability. All study data are included in this article and/or *SI Appendix*. Raw data and associated R codes are available at <https://github.com/DanielRAmor/Fast-growth-can-counteract-susceptibility>.

ACKNOWLEDGMENTS. We thank the members of the Gore Laboratory for feedback, with special thanks to Christoph Ratzke, Martina Dal Bello, and Jonathan Friedman. D.R.A. acknowledges the support of the Field of Excellence ‘‘Complexity in Life, Basic Research and Innovation’’ at University of Graz. The authors also acknowledge support from NIH Grant R01-GM102311 and the Schmidt Science Polymath Award.

Author affiliations: ^aPhysics of Living Systems, Department of Physics, Massachusetts Institute of Technology, Cambridge, MA 02139

- P. I. Costea *et al.*, Enterotypes in the landscape of gut microbial community composition. *Nat. Microbiol.* **3**, 8–16 (2018).
- J. Zhou *et al.*, Stochastic assembly leads to alternative communities with distinct functions in a bioreactor microbial community. *MBio* **4**, e00584-12 (2013).
- G. E. Leventhal *et al.*, Strain-level diversity drives alternative community types in millimetre-scale granular biofilms. *Nat. Microbiol.* **3**, 1295–1303 (2018).
- J. Friedman, L. M. Higgins, J. Gore, Community structure follows simple assembly rules in microbial microcosms. *Nat. Ecol. Evol.* **1**, 0109 (2017).
- L. Lahti, J. Salojärvi, A. Salonen, M. Scheffer, W. M. de Vos, Tipping elements in the human intestinal ecosystem. *Nat. Commun.* **5**, 4344 (2014).
- C. Tropini *et al.*, Transient osmotic perturbation causes long-term alteration to the gut microbiota. *Cell* **173**, 1742–1754.e17 (2018).
- S. Estrela *et al.*, Functional attractors in microbial community assembly. *Cell Systems* **13**, 29–42.e7 (2022).
- R. Levy *et al.*, Longitudinal analysis reveals transition barriers between dominant ecological states in the gut microbiome. *Proc. Natl. Acad. Sci. U.S.A.* **117**, 13839–13845 (2020).
- L. Dethlefsen, D. A. Relman, Incomplete recovery and individualized responses of the human distal gut microbiota to repeated antibiotic perturbation. *Proc. Natl. Acad. Sci. U.S.A.* **108**, 4554–4561 (2011).
- L. A. David *et al.*, Host lifestyle affects human microbiota on daily timescales. *Genome Biol.* **15**, R89 (2014).
- A. M. Seekatz, K. Rao, K. Santhosh, V. B. Young, Dynamics of the fecal microbiome in patients with recurrent and nonrecurrent *Clostridium difficile* infection. *Genome Med.* **8**, 47 (2016).
- M. Cycoń, A. Mroziak, Z. Piotrowska-Seget, Antibiotics in the soil environment—Degradation and their impact on microbial activity and diversity. *Front. Microbiol.* **10**, 338 (2019).
- D. R. Amor, C. Ratzke, J. Gore, Transient invaders can induce shifts between alternative stable states of microbial communities. *Sci. Adv.* **6**, eaay8676 (2020).
- V. Dubinkina, Y. Fridman, P. P. Pandey, S. Maslov, Multistability and regime shifts in microbial communities explained by competition for essential nutrients. *eLife* **8**, e49720 (2019).
- J. Guittar, T. Koffel, A. Shade, C. A. Klausmeier, E. Litchman, Resource competition and host feedbacks underlie regime shifts in gut microbiota. *Am. Nat.* **198**, 1–12 (2021).
- E. W. Jones, J. M. Carlson, Steady-state reduction of generalized Lotka-Volterra systems in the microbiome. *Phys. Rev. E* **99**, 032403 (2019).
- M. Scheffer, *Critical Transitions in Nature and Society* (Princeton University Press, 2009).
- R. I. Aminov, A brief history of the antibiotic era: Lessons learned and challenges for the future. *Front. Microbiol.* **1**, 134 (2010).
- A. Brauner, O. Fridman, O. Gefen, N. Q. Balaban, Distinguishing between resistance, tolerance and persistence to antibiotic treatment. *Nat. Rev. Microbiol.* **14**, 320–330 (2016).
- L. Dethlefsen, S. Huse, M. L. Sogin, D. A. Relman, The pervasive effects of an antibiotic on the human gut microbiota, as revealed by deep 16S rRNA sequencing. *PLoS Biol.* **6**, e280 (2008).
- L. P. Shaw *et al.*, Modelling microbiome recovery after antibiotics using a stability landscape framework. *ISME J.* **13**, 1845–1856 (2019).
- H. R. Meredith, J. K. Srimani, A. J. Lee, A. J. Lopatkin, L. You, Collective antibiotic tolerance: Mechanisms, dynamics and intervention. *Nat. Chem. Biol.* **11**, 182–188 (2015).
- M. G. J. de Vos, M. Zagorski, A. McNally, T. Bollenbach, Interaction networks, ecological stability, and collective antibiotic tolerance in polymicrobial infections. *Proc. Natl. Acad. Sci. U.S.A.* **114**, 10666–10671 (2017).
- R. S. McInnes, G. E. McCallum, L. E. Lamberte, W. van Schaik, Horizontal transfer of antibiotic resistance genes in the human gut microbiome. *Curr. Opin. Microbiol.* **53**, 35–43 (2020).
- D. Rodríguez Amor, M. Dal Bello, Bottom-up approaches to synthetic cooperation in microbial communities. *Life (Basel)* **9**, E22 (2019).
- E. A. Yurtsev, H. X. Chao, M. S. Datta, T. Artemova, J. Gore, Bacterial cheating drives the population dynamics of cooperative antibiotic resistance plasmids. *Mol. Syst. Biol.* **9**, 683 (2013).
- R. A. Sorg *et al.*, Collective resistance in microbial communities by intracellular antibiotic deactivation. *PLoS Biol.* **14**, e2000631 (2016).
- L. Galera-Laporta, J. Garcia-Ojalvo, Antithetic population response to antibiotics in a polybacterial community. *Sci. Adv.* **6**, eaaz5108 (2020).
- N. M. Vega, J. Gore, Collective antibiotic resistance: Mechanisms and implications. *Curr. Opin. Microbiol.* **21**, 28–34 (2014).
- A. Shade *et al.*, Fundamentals of microbial community resistance and resilience. *Microbiol.* **3**, 417 (2012).
- H. R. Meredith *et al.*, Applying ecological resistance and resilience to dissect bacterial antibiotic responses. *Sci. Adv.* **4**, eaau1873 (2018).
- F. T. De Vries *et al.*, Land use alters the resistance and resilience of soil food webs to drought. *Nat. Clim. Chang.* **2**, 276–280 (2012).
- S. L. Tuck *et al.*, The value of biodiversity for the functioning of tropical forests: Insurance effects during the first decade of the Sabah biodiversity experiment. *Proc. R. Soc. B Biol. Sci.* **283**, 20161451 (2016).
- R. D. Bardgett, T. Caruso, Soil microbial community responses to climate extremes: Resistance, resilience and transitions to alternative states. *Philos. Trans. R. Soc. B Biol. Sci.* **375**, 20190112 (2020).

35. A. Aranda-Díaz *et al.*, Bacterial interspecies interactions modulate pH-mediated antibiotic tolerance. *eLife* **9**, e51493 (2020).
36. A. Chen, A. Sanchez, L. Dai, J. Gore, Dynamics of a producer-freeloader ecosystem on the brink of collapse. *Nat. Commun.* **5**, 3713 (2014).
37. E. M. Adamowicz, J. Flynn, R. C. Hunter, W. R. Harcombe, Cross-feeding modulates antibiotic tolerance in bacterial communities. *ISME J.* **12**, 2723–2735 (2018).
38. C. Ratzke, J. Gore, Modifying and reacting to the environmental pH can drive bacterial interactions. *PLoS Biol.* **16**, e2004248 (2018).
39. C. I. Abreu, J. Friedman, V. L. Andersen Woltz, J. Gore, Mortality causes universal changes in microbial community composition. *Nat. Commun.* **10**, 2120 (2019).
40. J. Clobert, M. Baguette, T. G. Benton, J. M. Bullock, Dispersal Ecology and Evolution. *Dispersal Ecol. Evol.* (OUP, 2012).
41. M. Derrien, J. E. T. van Hylckama Vlieg, Fate, activity, and impact of ingested bacteria within the human gut microbiota. *Trends Microbiol.* **23**, 354–366 (2015).
42. S. A. Levin, Dispersion and population interactions. *Am. Nat.* **108**, 207–228 (1974).
43. T. Fukami, Integrating internal and external dispersal in metacommunity assembly: Preliminary theoretical analyses. *Ecol. Res.* **20**, 623–631 (2005).
44. R. V. Solé, D. Alonso, A. McKane, Self-organized instability in complex ecosystems. *Philos. Trans. R. Soc. Lond. B Biol. Sci.* **357**, 667–671 (2002).
45. F. Roy, M. Barbier, G. Biroli, G. Bunin, Complex interactions can create persistent fluctuations in high-diversity ecosystems. *PLoS Comput. Biol.* **16**, e1007827 (2020).
46. M. T. Pearce, A. Agarwala, D. S. Fisher, Stabilization of extensive fine-scale diversity by ecologically driven spatiotemporal chaos. *Proc. Natl. Acad. Sci. U.S.A.* **117**, 14572–14583 (2020).
47. B. G. Weiner, A. Posfai, N. S. Wingreen, Spatial ecology of territorial populations. *Proc. Natl. Acad. Sci. U.S.A.* **116**, 17874–17879 (2019).
48. R. Smith *et al.*, Programmed Allee effect in bacteria causes a tradeoff between population spread and survival. *Proc. Natl. Acad. Sci. U.S.A.* **111**, 1969–1974 (2014).
49. S. Hromada *et al.*, Negative interactions determine *Clostridioides difficile* growth in synthetic human gut communities. *Mol. Syst. Biol.* **17**, e10355 (2021).
50. S. Evans, J. B. H. Martiny, S. D. Allison, Effects of dispersal and selection on stochastic assembly in microbial communities. *ISME J.* **11**, 176–185 (2017).
51. N. M. Vega, J. Gore, Stochastic assembly produces heterogeneous communities in the *Caenorhabditis elegans* intestine. *PLoS Biol.* **15**, e2000633 (2017).
52. B. Obadia *et al.*, Probabilistic invasion underlies natural gut microbiome stability. *Curr. Biol.* **27**, 1999–2006.e8 (2017).
53. J. Cairns, R. Jokela, L. Becks, V. Mustonen, T. Hiltunen, Repeatable ecological dynamics govern the response of experimental communities to antibiotic pulse perturbation. *Nat. Ecol. Evol.* **4**, 1385–1394 (2020).
54. M. Rajilić-Stojanović, W. M. de Vos, The first 1000 cultured species of the human gastrointestinal microbiota. *FEMS Microbiol. Rev.* **38**, 996–1047 (2014).
55. H. A. Seddik *et al.*, *Lactobacillus plantarum* and its probiotic and food potentialities. *Probiotics Antimicrob. Proteins* **9**, 111–122 (2017).
56. J. Suez *et al.*, Post-antibiotic gut mucosal microbiome reconstitution is impaired by probiotics and improved by autologous FMT. *Cell* **174**, 1406–1423.e16 (2018).
57. B. A. Lipsky, A. C. Goldberger, L. S. Tompkins, J. J. Plorde, Infections caused by nondiphtheria corynebacteria. *Rev. Infect. Dis.* **4**, 1220–1235 (1982).
58. F. Enam, T. J. Mansell, Prebiotics: Tools to manipulate the gut microbiome and metabolome. *J. Ind. Microbiol. Biotechnol.* **46**, 1445–1459 (2019).
59. C. M. Taylor, A. Hastings, Allee effects in biological invasions. *Ecol. Lett.* **8**, 895–908 (2005).
60. E. A. Anisimova, D. R. Yarullina, Antibiotic resistance of *Lactobacillus* strains. *Curr. Microbiol.* **76**, 1407–1416 (2019).
61. O. Fridman, A. Goldberg, I. Ronin, N. Shores, N. Q. Balaban, Optimization of lag time underlies antibiotic tolerance in evolved bacterial populations. *Nature* **513**, 418–421 (2014).
62. A. Ortiz, N. M. Vega, C. Ratzke, J. Gore, Interspecies bacterial competition regulates community assembly in the *C. elegans* intestine. *ISME J.* **15**, 2131–2145 (2021).